Arc Light Sensing of Droplet Transfer and its Analysis in Pulsed GMAW Process

A novel arc light sensing method for droplet transfer has been developed and an arc light radiant flux signal of droplet detachment is described

BY Q. L. WANG AND P. J. LI

ABSTRACT. A new method and its principle for sensing droplet transfer in GMAW of steel and aluminum alloy have been researched in this paper. A practical arc light sensing and controlling system has been developed. The reliability of the arc light characteristic signal that indicates droplet detachment and the control accuracy of the system have been verified using high-speed photography. Based on the mathematical model established in the paper, the mechanism of the signal and relative phenomena were analyzed. The parameters that influence arc light radiation were given and the limitation of this sensing method was discussed.

Introduction

Gas metal arc welding has made rapid progress in recent decades. However, consistency of the resultant weld quality, which is closely related to the stability of droplet transfer, is yet to be researched.

The introduction of pulsed GMAW offered the opportunity to conveniently control droplet transfer and one pulse one droplet (OPOD) transfer mode is generally recognized as the optimum transfer mode (Refs. 1–6). A significant number of works have been published on methods that can provide transfer mode when welding parameters are kept constant. However, these preliminary works are limited to the preset welding parameters obtained through experimentation or theoretical calculation (Refs. 5, 7–12). It is known as one-knob open-loop control.

Q. L. WANG is a Professor and President, and P. J. LI is a lecturer with the Department of Welding Engineering, Harbin Institute of Technology, Harbin, P. R. China.

It is known, however, that it is difficult to keep welding parameters (especially wire feed speed and arc length) constant during welding. For this reason, adaptive control systems with feedback control of some welding parameters have been developed (Refs. 2–6). The direct objective of adaptive control is not to control the droplet transfer. Therefore, it is still a type of open-loop control and impossible to provide reliable OPOD transfer. In order to control the droplet transfer directly, the only feasible way is to find reliable sensing methods for droplet transfer.

High-speed photography and optical imaging are reliable methods for observing droplet transfer; however, presently they are not suitable for the real-time sensing and control of droplet transfer. A number of works on other sensing methods, such as acoustic emission and arc sound sensing, have been presented (Refs. 13–17), but they have all been very susceptible to ambient noise. The electrical signal sensing method (arc voltage, welding current) (Refs. 2, 8, 14, 16, and 18–26) is only effective for the short circuit transfer and globular transfer processes, but not for the spray transfer process, because the signal-to-noise ratio is too low (for example, $0.5\ V < \Delta V < 1\ V$).

Arc light sensing is a promising method for sensing droplet transfer, and has already been used by some researchers (Refs. 18, 27). However, the following problems still exist:

1) The signal-to-noise ratio of the arc light signal is comparatively low;

2) Some of the previous works only addressed the spray transfer in constant voltage welding, not the OPOD transfer;

3) The sensors are impractical, *i.e.*, difficult to adjust, clumsy or expensive.

The purpose of the work presented in this paper is to develop a novel practical arc light sensing and control system, and to explore the physical essence of arc light signal variation during projected droplet transfer in pulsed GMAW of steel and aluminum alloy.

KEY WORDS

GMAW
Droplet Transfer
Arc Light Sensor
OPOD Control
Steel GMAW
Aluminum GMAW
Arc Radiant
Close-loop Control

Experimental Procedure

All experiments were performed with bead-on-plate welding. Mild steel (AWS ER70s-3) and aluminum alloy (AA1100) workpieces were, respectively, 250 x 80 x 10 mm and 200 x 100 x 5 mm. In steel welding, 1.2-mm-diameter steel welding wire (AWS ER70S) was used and the shielding gases were pure argon and argon-rich gas (Ar-CO_2, Ar-O_2) with a flow rate of 15 L/min. In aluminum welding, 1.6-mm-diameter aluminum alloy welding wire (AA4043) was used and the shielding gas was pure argon with a flow rate of 25 L/min.

The main welding equipment was a transistor welding power supply MM350 (OCR), a Miller wire feeder (S-54D) for steel and a Planetic wire feeder (Mercury 501) for aluminum. The power supply provided a total peak output current of over 450 A. In pulse mode, the background current was 50 A. Due to the switching action of power transistors, the output ripple of the power supply was significant, as shown in Fig. 1. A transversing weld table was used so the weld gun could remain fixed.

Analysis of metal transfer was performed using high-speed photography (using an NAC-16D type high-speed camera) with a xenon backlight. The arc image and arc light sensing signal waveform were recorded on one frame using a synchronous imaging method.

The arc light sensor, with dimensions of 15 mm in diameter and 50 mm in length, was clamped on the welding torch — Fig. 2. The light sensitive component is phototriode and the sensor worked well under any practical conditions with some protective design. In order to enlarge its dynamic range, a special control circuit was used. This circuit can adjust the sensitivity of phototriode according to the arc light intensity automatically.

For practical application, a Philips single chip microcomputer 80C552 (main frequency 16 MHz) was used in the sensing and control system. It received the arc light signal from the sensor and at the same time controlled the welding power source and wire feeder. It was also capable of sampling, processing data and judging droplet detachment, etc. Data could be transferred to a personal computer for further analysis. The welding parameters used as variables in the experiments were peak current, pulse frequency, shielding gas composition and contact-tube-to-work distance. Some of the experiments were performed on flat workpieces; others were performed on specially shaped workpieces. All experiments were performed with automatic bead-on-plate welding. Figure 3 shows the overall layout of the experimental equipment. The purpose of the following experiments was to study the relationship between the arc light signal and the droplet detachment.

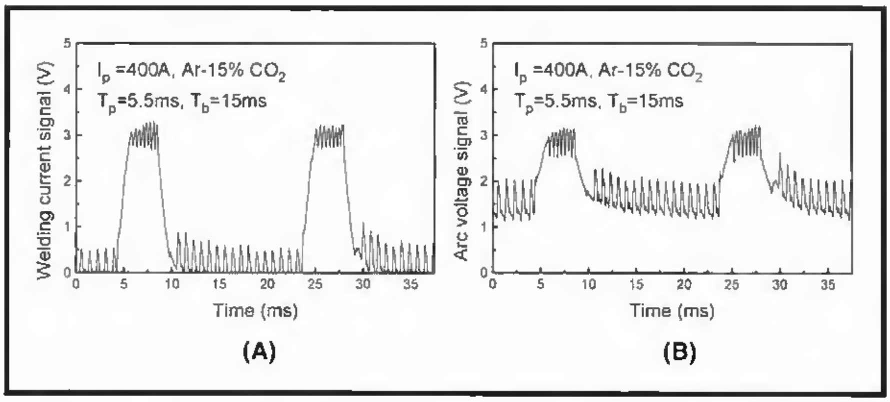

Fig. 1 — The output waveforms of the welding power source. A — Current waveform; B — voltage waveform.

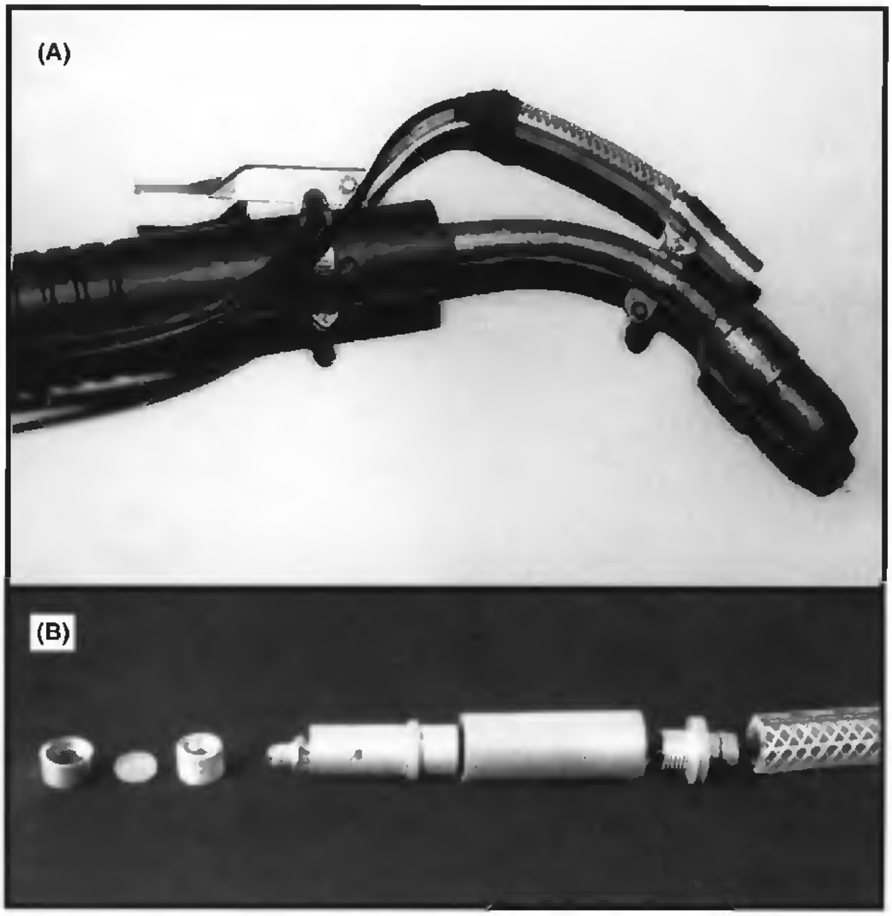

Fig. 2 — The arc light sensor. A — Clamped on a semiautomatic welding gun; B — internal structure.

Pulsed GMAW of Steel

Droplet detachment is not clearly indicated in the electrical signal under spray transfer mode (Fig. 1), but is clearly indicated in the arc light radiant flux signal (Fig. 4A and B), with argon-rich shielding. The significant decrease in the arc light radiant flux signal corresponds to the droplet detachment. It has been proven indirectly in previous work (Ref. 27), and proven directly by high-speed photograph, and synchronic signal waveform (Fig. 5) in this paper. To clearly show the variation in the arc light signal on the film, only part of the signal blocked with dot-dash lines in Fig. 5 is taken. It can be seen that the decrease in the arc light radiant flux signal strictly corresponds with the droplet detachment. The reliability of this phenomenon was proven by repeated experiments and the signal-to-noise ratio of the sensing method was high despite the large ripple on the output current of the welding power source.

However, the arc light radiant flux signal cannot indicate droplet detachment in pulsed GMAW of steel shielded with pure argon—Fig. 4C. The reason for this phenomenon will be given in the discussion of this paper.

Pulsed GMAW of Aluminum Alloy

As shown in Fig. 4D, an obvious decrease in the arc light radiant flux signal also occurs in pulsed GMAW of aluminum alloy. High-speed photography illustrates that the decrease in arc light signal strictly corresponds to droplet de-

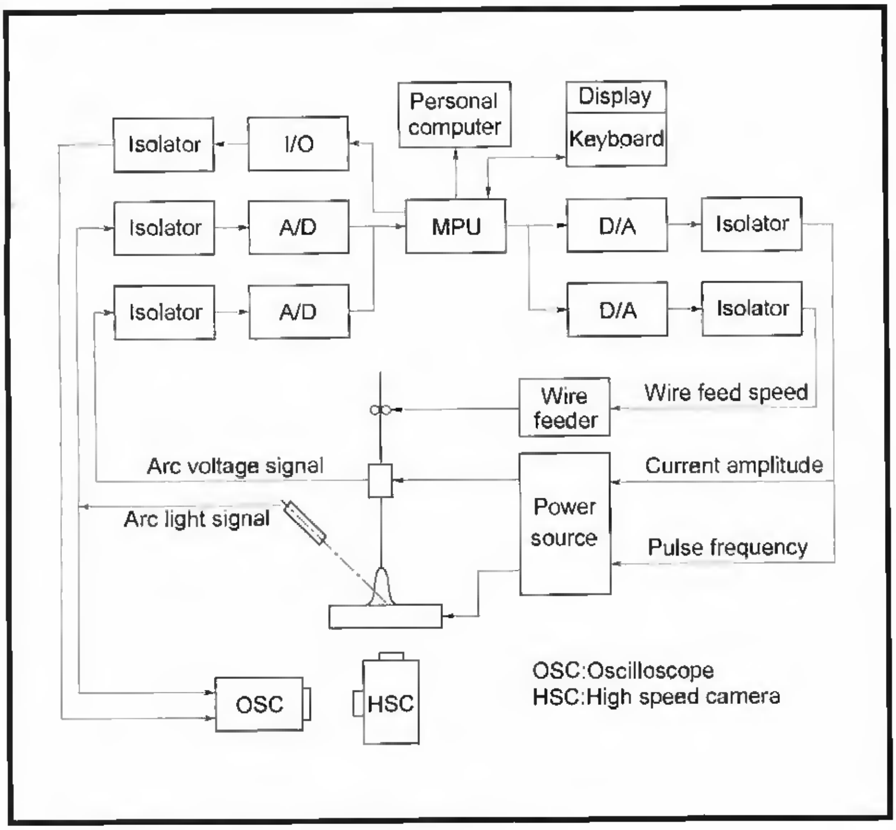

Fig. 3 — The overall layout of the experimental equipment.

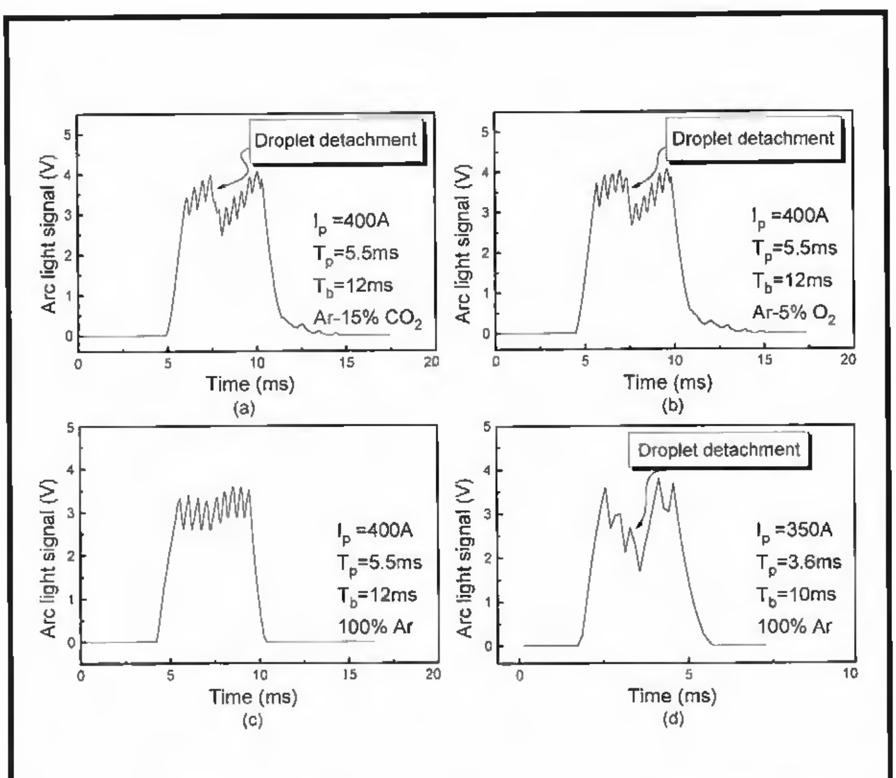

Fig. 4 — Signals of arc light radiant flux in pulsed GMAW of steel and aluminum alloy. A — Steel, Ar-15%CO_2; B — steel, Ar-5%O_2; C — steel, Ar; D — aluminum, Ar.

tachment, as shown in Fig. 6. The sensing signal was proven reliable and of high signal-to-noise ratio through repeated experiments.

Closed-Loop Control of Droplet Transfer in Pulsed GMAW of Steel

On the basis of the relationship between the variation of the arc light radiant flux signal and droplet detachment, a closed-loop control system for the droplet transfer process in steel welding was developed. The pulse peak current amplitude was set to 400 A. As shown in Fig. 7, during peak current time, as soon as the decrease in arc light exceeded the threshold selected through experimentation, a control signal was sent to the welding power source and the welding current immediately changed to background current. Neither streaming due to surplus pulse energy nor globular transfer due to lack of pulse energy occurred. Using an MCS-51 language control program we developed ourselves, the whole judgment time (including time of sampling, calculating to detect droplet detachment and sending the control signal if droplet detachment occurs) was less than 190 μs. Thus, the feedback loop frequency of this control exceeds 5000 times per second and this high frequency can guarantee the accurate control of droplet transfer. In the pulse peak current time, the average value of arc light signal was calculated. This value has a reliable linear relation with arc length. Therefore, arc length can be calculated from this value. A PID feedback mechanism is used in arc length control during background current time, the calculating time of which is less than 2.4 ms. Background current amplitude is fixed at 50 A. The background current time is calculated with PID calculation and adjusted to maintain the constant arc length. After setting peak current, wire feed speed and arc voltage, the pulse peak current time and background current time will be automatically adjusted by control system to maintain OPOD transfer mode and constant arc length. The reliability of the control process was improved by using relative threshold (15% of the average value of arc light radiant flux signal during peak current). Although the absolute arc light signal value changes correspondingly when arc length changes within the range of 3 through 12 mm, the control system is capable of maintaining OPOD transfer mode reliably. Figure 8 shows the close-loop control process of pulsed GMAW of steel. Based on a number of high-speed photographs of control experiments, the reliability of

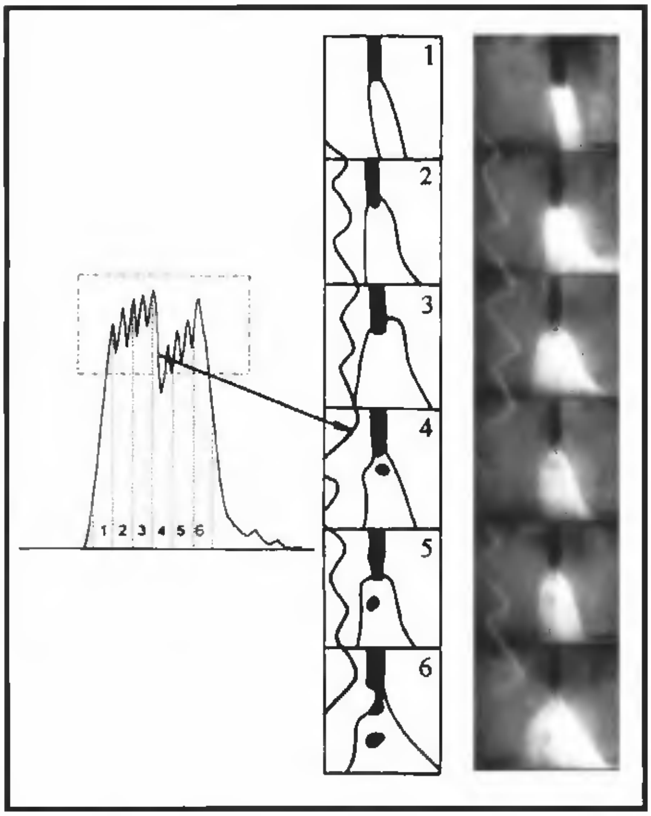

Fig. 5 — The high-speed photographs of droplet transfer in pulsed GMAW of steel (1000 frames per second): Ip = 400 A, Tp = 5.5 ms, Tb = 12 ms, Ar-15%CO_2.

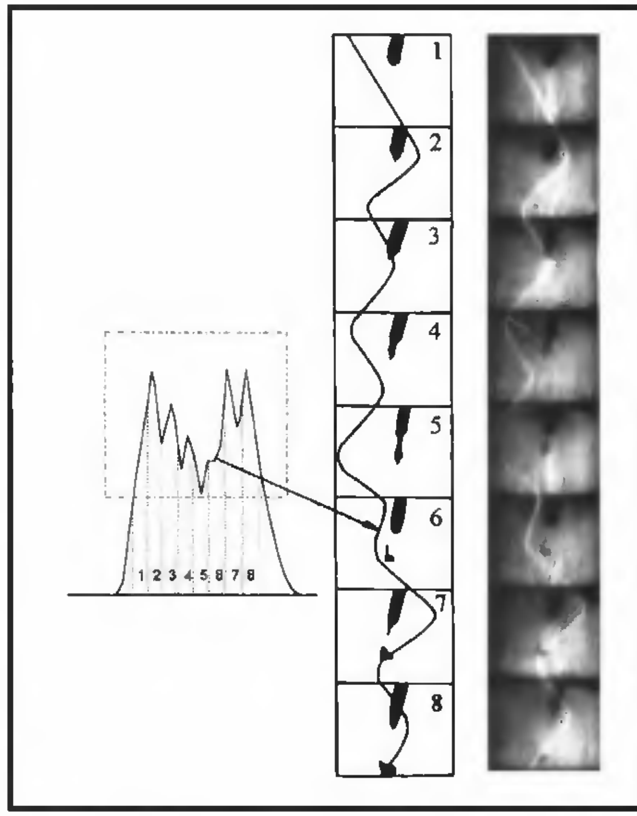

Fig. 6 — The high-speed photographs of droplet transfer in pulsed GMAW of aluminum alloy (3000 frames per second): Ip = 350 A, Tp = 3.5 ms, Tb = 10 ms, 100% Ar.

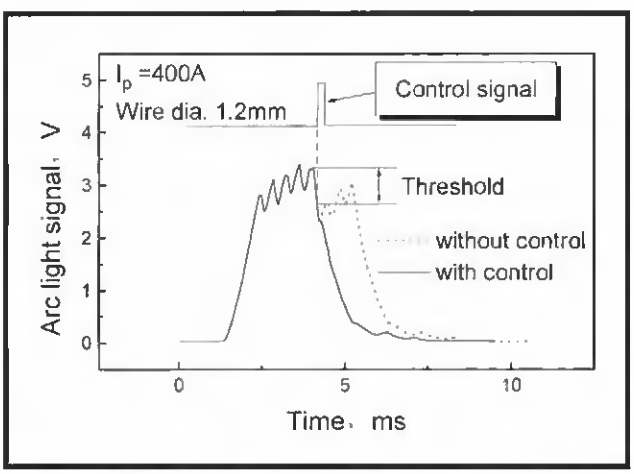

Fig. 7 — Schematic of droplet detaching judgment in pulsed GMAW of steel.

the system in detecting droplet detachment has been proven to be 96%. Error mainly resulted from the large ripple of the welding power source output. The maximal pulse frequency we used with this system was 130 Hz and droplet detachment was detected reliably.

Figure 9 is the photograph of bead formation of steel under droplet transfer closed-loop control. The bead profile is very regular and its ripple is very small, free from traces of spatter. The droplet transfer closed-loop control system for aluminum alloy is being evaluated now.

Analysis of the Arc Light Signal

Physical Essence and Influencing Factors of Arc Light Radiation

In GMAW with high welding current (more than 100 A), the arc plasma is in local thermodynamic equilibrium (LTE) condition (Refs. 28, 29). In this case, the Kirchhoff rule can be used to calculate the spectrum intensity B_v of the arc plasma (Refs. 30–32):

$$B_v = \frac{2\cdot h\cdot v^3}{c^2\cdot e^{\frac{h\cdot v}{k\cdot T_e}}-1} \tag{1}$$

where B_v is the radiosity of unit stereo angle and unit frequency interval, c is light velocity, T_e is electron temperature, v is frequency and k is boltzman constant. It is now assumed that arc light radiance is isotropic, then the radiosity U_v can be represented by:

$$U_v = \frac{4\pi}{c}B_v \tag{2}$$

The sensitive spectrum range of the sensor used in this work is narrow. The peak sensitive wave length is 820 nm. In this case, $hv/kt<<1$, the condition of Rayleigh-Jeans approximation is fulfilled, Equation 2 is approximately equal to:

$$U_v = 8\pi\frac{v^2}{c^3}kT_e \tag{3}$$

Under atmospheric pressure and with high current, the electron temperature is approximately equal to arc temperature (Ref. 30). It is now assumed that heat losses are all due to conduction (Ref. 30), then the Elenbass-Heller rule (Ref. 31) is fulfilled:

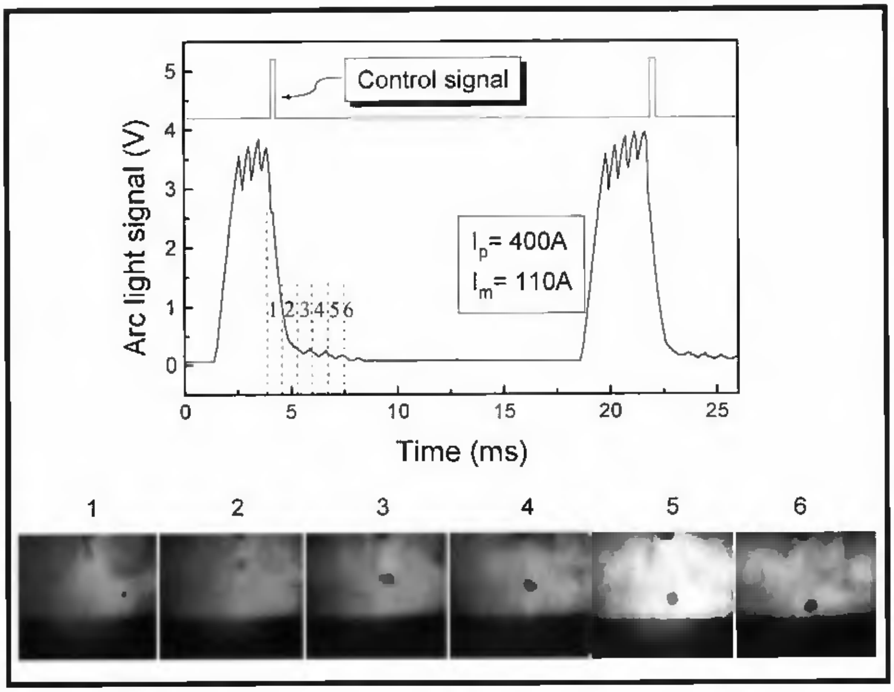

Fig. 8 — The high-speed photograph of droplet transfer with OPOD control in pulsed GMAW of steel.

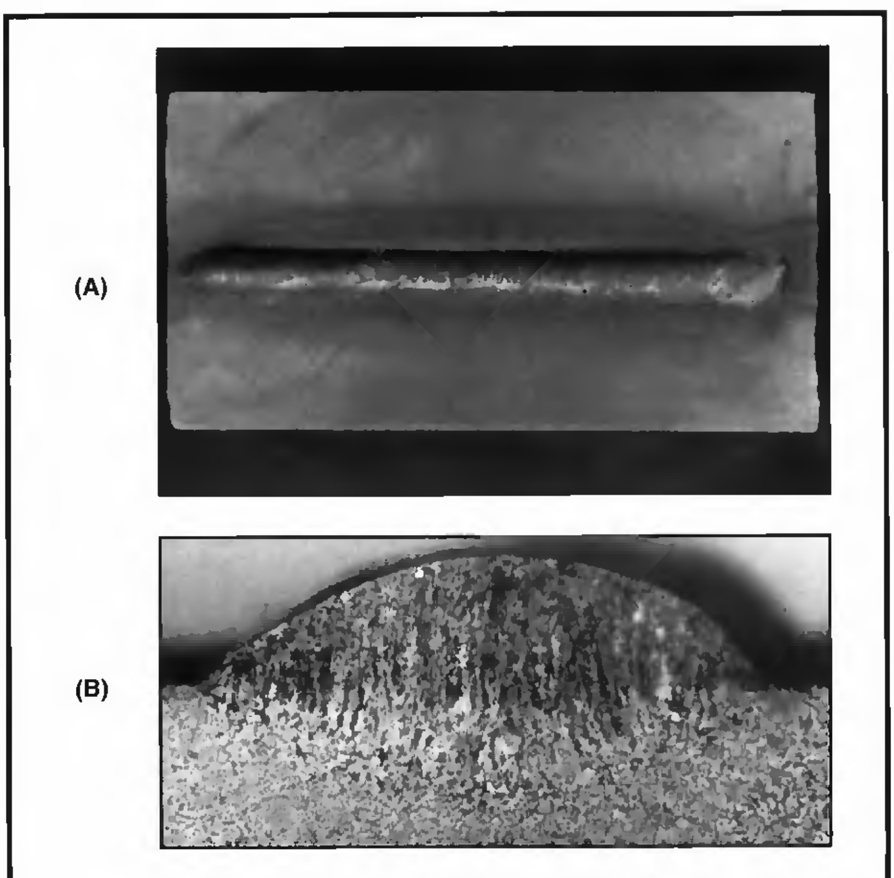

Fig. 9 — The weld bead with OPOD control in pulsed GMAW of steel. A — Front side; B — cross section.

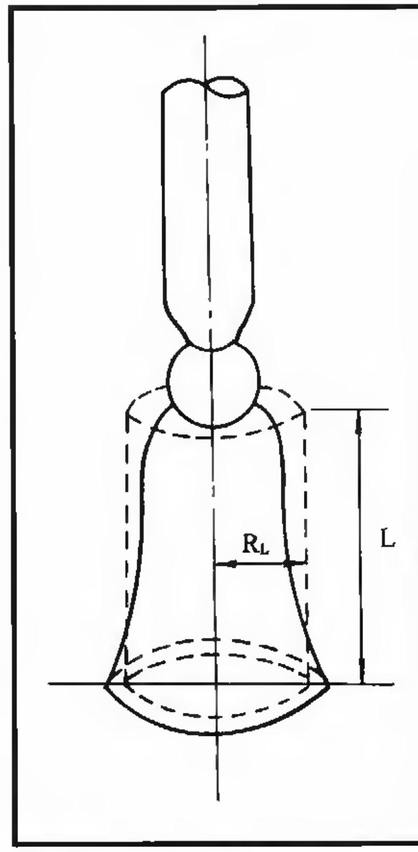

Fig. 10 — The sketch of the arc plasma luminary.

$$\sigma E^2 + \frac{1}{r} d\left(\frac{r\lambda dT}{dr}\right) / dr = 0 \qquad (4)$$

where E is the voltage gradient of arc, r is radius, λ is thermal conductivity and σ is electric conductivity. As shown in Fig. 10, we can assume arc plasma luminary as a column, R_L in radius and L in length. With derivation in the Appendix the mathematical model of arc radiant energy can be represented by:

$$U = 8\pi k \frac{v^2}{c^3} \left\{ IEL\left[\left(\frac{1}{4} - \frac{\ln R_L}{2}\right) R_L^2 + \left(\frac{\ln r_a}{2} - \frac{3}{8}\right) r_a^2 \right] + \pi C_2 L R_L^2 + \pi C_3 L r_a^2 \right\} + C \qquad (5)$$

where r_a is the radius of electric conducting area and C, C_2 and C_3 are constants. Equation 5 shows that the direct influencing factors of arc radiation include welding current I, voltage gradient of arc E, arc length L and the radius of plasma luminary R_L.

The Relationship Between Arc Light Radiant Signal and Arc Plasma Luminary Geometry

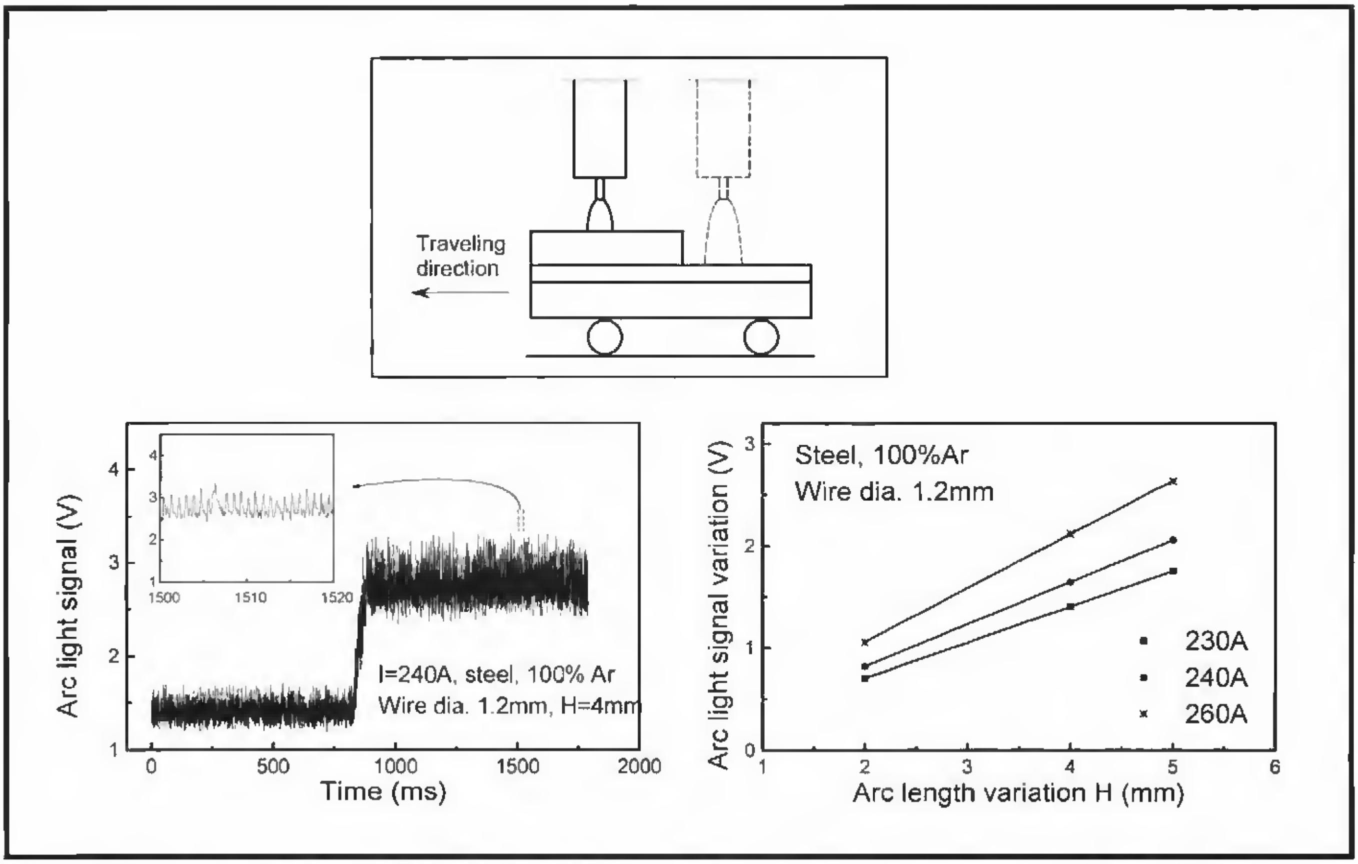

Fig. 11 — Schematic of experiment with step-shaped workpiece and the relationship between the arc light radiant flux signal and the height of the step with different welding currents.

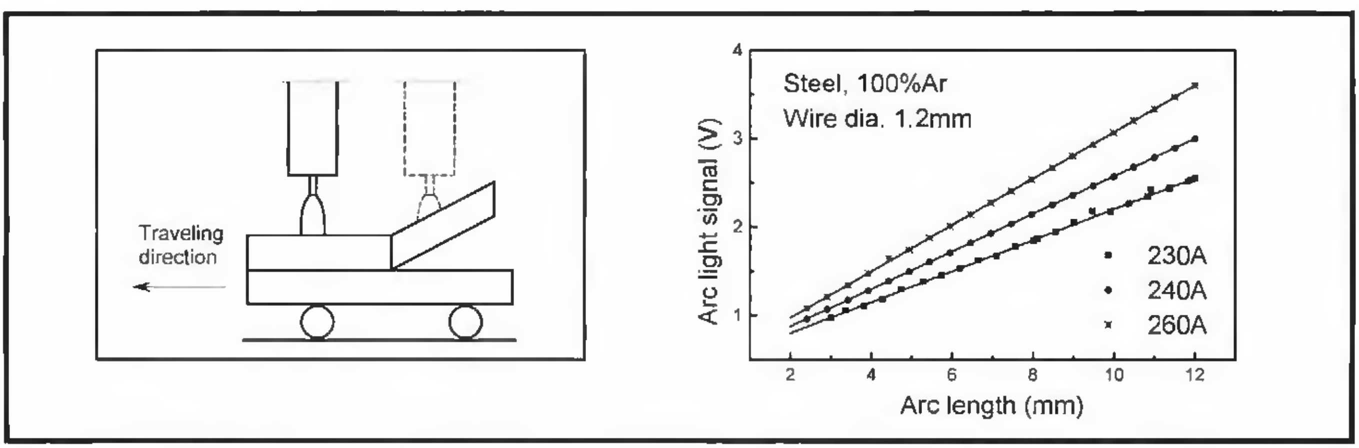

Fig. 12 — Schematic of experiment with slope-shaped workpiece and the relationship between the arc light radiant flux signal and the arc length with different welding currents.

Dimension (Arc Length L, Radius R_L)

Equation 5 shows that both welding regime and arc plasma luminary geometric dimensions influence the arc light radiation. However, under spray transfer mode, no obvious variation occurs in welding current and voltage signal, as shown in Fig. 1. It can be deduced that the decrease in arc light radiant flux signal, which indicates droplet transfer, results from the geometric dimension variation due to the droplet detachment. The next two groups of experiments were designed to demonstrate this deduction.

The Effect of Variation in Arc Length (L)

Specially shaped workpieces were used in this group of experiments, as shown in Figs. 11 and 12. The shielding gas was pure argon. Welding current range was 230 through 260 A. Constant current output characteristic of the welding power supply was used to keep the current constant when arc length changed. The travel speed of the transversing table was set as high as possible (60 cm/min) to eliminate the arc self adjustment. Figure 11 shows the arc light variation in the experiments using step-shaped workpieces. The fluctuation of arc light signal is due to the welding cur-

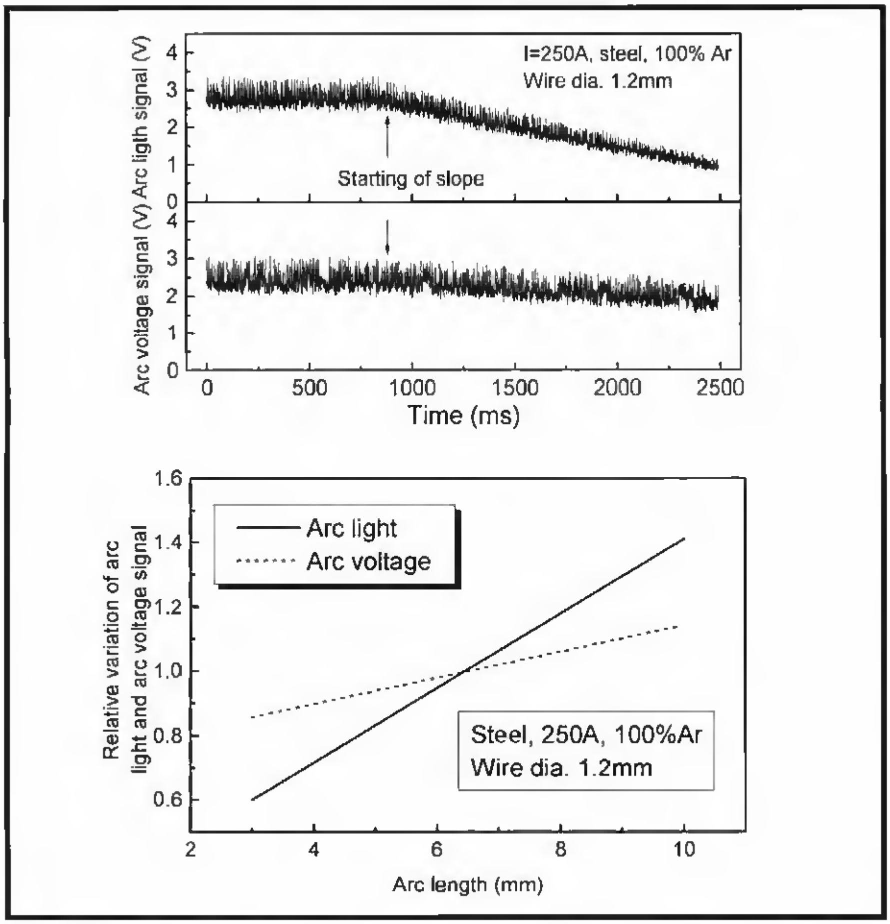

Fig. 13 — The absolute and relative variation between arc voltage and arc light radiant flux signal vs. arc length.

rent ripple. The height of the step and the welding current were variables in the experiments. As the arc length increases for a given current, a linear increase in arc light signal occurs. As the current increased, the velocity of the arc light signal became increasingly higher. The variation of arc light radiant flux signal $\Delta\Phi$ can be regressed to an equation correlating with arc length and current:

$$\Delta\Phi = k_1 \cdot I \cdot H + k_2 \cdot H \qquad (6)$$

where k_1, k_2 are constants, H is the step height, I is the current. For I in A, L in mm, $\Delta\Phi$ in V, the coefficients in this equation were $k_1 = 0.002975$ and $k_2 = -0.50834$.

In the experiments using slope-shaped workpieces, welding current range was 230 through 260 A. As the arc length increased for a given current, a linear increase in arc light signal occurred, as shown in Fig. 12. The arc light signals were regressed to an expression correlating with the arc length and current:

$$\Phi = P_1 \cdot I \cdot L + P_2 \cdot L + P_3 \qquad (7)$$

where Φ was arc light radiant flux signal and P_1, P_2, P_3 were constants. For current in A, arc length in mm, arc light signal in V, the coefficients were $P_1 = 0.002875$, $P_2 = -0.428$ and $P_3 = 0.576$. The maximum relative deviation was 8%. The experiments were performed under streaming transfer mode with stable arc profile. If the radius of plasma luminary is defined as a constant, the mathematical model represented by Equation 5 could be converted into the same pattern as Equation 7. T. A. Siewert drew the same conclusion using statistics from a large amount of experimental results (Ref. 23). Figure 13 shows the experiment data and relative variation of arc voltage and arc light signal vs. arc length variation in experiments with slope-shaped workpieces. Because the absolute values of arc light and arc voltage signal are different, the relative value of each signal is used to compare the sensitivity between them. The relative variation value of arc light signal is calculated by dividing instantaneous arc light signal value with the average value of arc light signal, so does arc voltage signal. It is obvious that arc light signal is more sensitive to arc length variation than arc voltage signal.

The experiment results discussed above also hold true for pulsed GMAW process of steel and aluminum alloy.

The Result of the Radius of Arc Plasma Luminary

The second group of experiments was also performed with steady current GMAW of steel. The range of the current was 220 through 260 A. A special sensor was used, which will be referred to as a "slot sensor," shown in Fig. 14. The original diameter of the slot sensor was 5 mm and

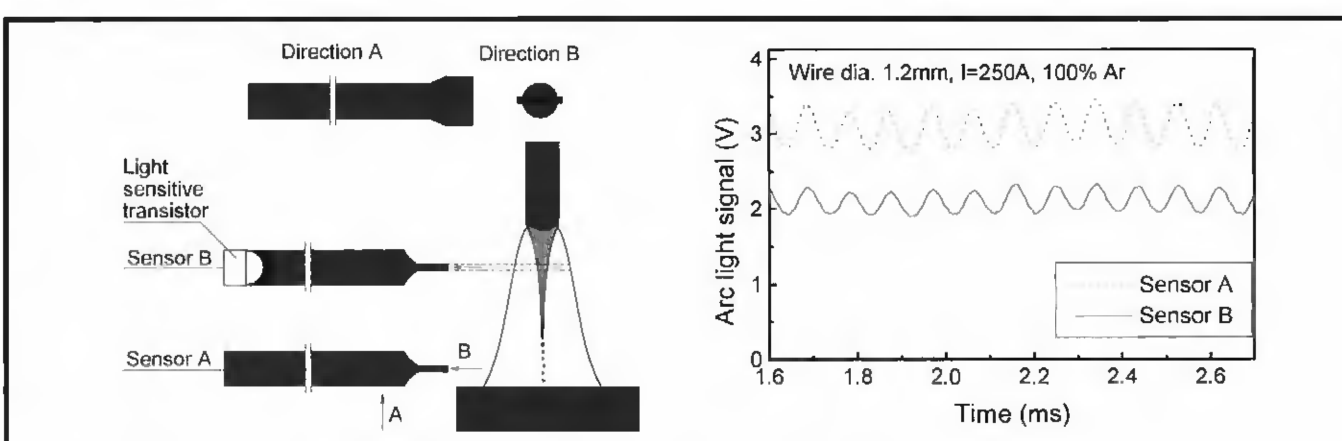

Fig. 14 — The influence of arc plasma luminary radius on arc light radiant flux signal.

the length was 12 mm. One tip of the sensor was pressed flat to form a slot, 0.5 mm in height and 7 mm in width. The view angle of the sensor is 1.5 deg. The internal surfaces of the sensors were made black to avoid unparallel incident light entering it. These sensors only received light emitted from the thin layer of plasma luminary in front of it. Two slot sensors were used to detect the arc light from different sections of the arc column. The absolute value of arc light signal corresponding to small luminary radius RL_1 was smaller than that of the larger luminary radius RL_2. The experiments demonstrated the relationship between arc light signal and arc plasma luminary radius. The experimental results qualitatively matched the mathematical model as well.

The Formation of the Characteristic Variation in Arc Light Radiant Flux Signal

In the first part of this work it was shown that the characteristic variation in arc light indicated droplet detachment. However, the mechanism of its formation is still unknown. It is necessary to make it clear for further study and application of this sensing method.

For this purpose, a special experiment was designed to sample the arc light signal from different parts along the axis of the arc and the arc light signal from the whole arc column synchronously. Through the comparison of the arc light signal of different parts of the arc and the analysis of the mathematical model, the formation of the characteristic signal was clarified.

As shown in Fig. 15, besides Sensor 1 used for detecting arc light radiant flux of the whole arc column, three slot sensors (Sensors 2, 3, and 4) were used at the same time to detect three different sections of the arc column along the axis of the arc. The arc light signal collected with these sensors is shown in Fig. 16. Arc light signal collected by Sensor 2 represented the variation in arc light radiant flux caused mainly by arc length variation. During the t1 period, the melting metal at the tip of the electrode formed a droplet and the arc length decreased with the elongation of the neck. Therefore, the amplitude of the arc light signal of steel and aluminum alloy welding process collected by Sensor 2 decreased gradually from the beginning of peak current time. During the t2 period, just before droplet detachment, the arc light flux signal reached a minimum value and rapidly increased after droplet detachment. During the t3 period, the plasma luminary enlarged gradually and the arc light radiant flux signal increased correspondingly. It can be seen from the Sensor 2 that, both in steel and in aluminum welding processes, the changes in arc length caused by droplet detachment results in the variations in arc light radiant flux signals. The tendency of these variations was almost the same. The arc light signals collected by Sensors 3 and 4 represent the influence of plasma luminary radius.

The appearances of these signals of steel and aluminum alloy welding processes were quite different from each

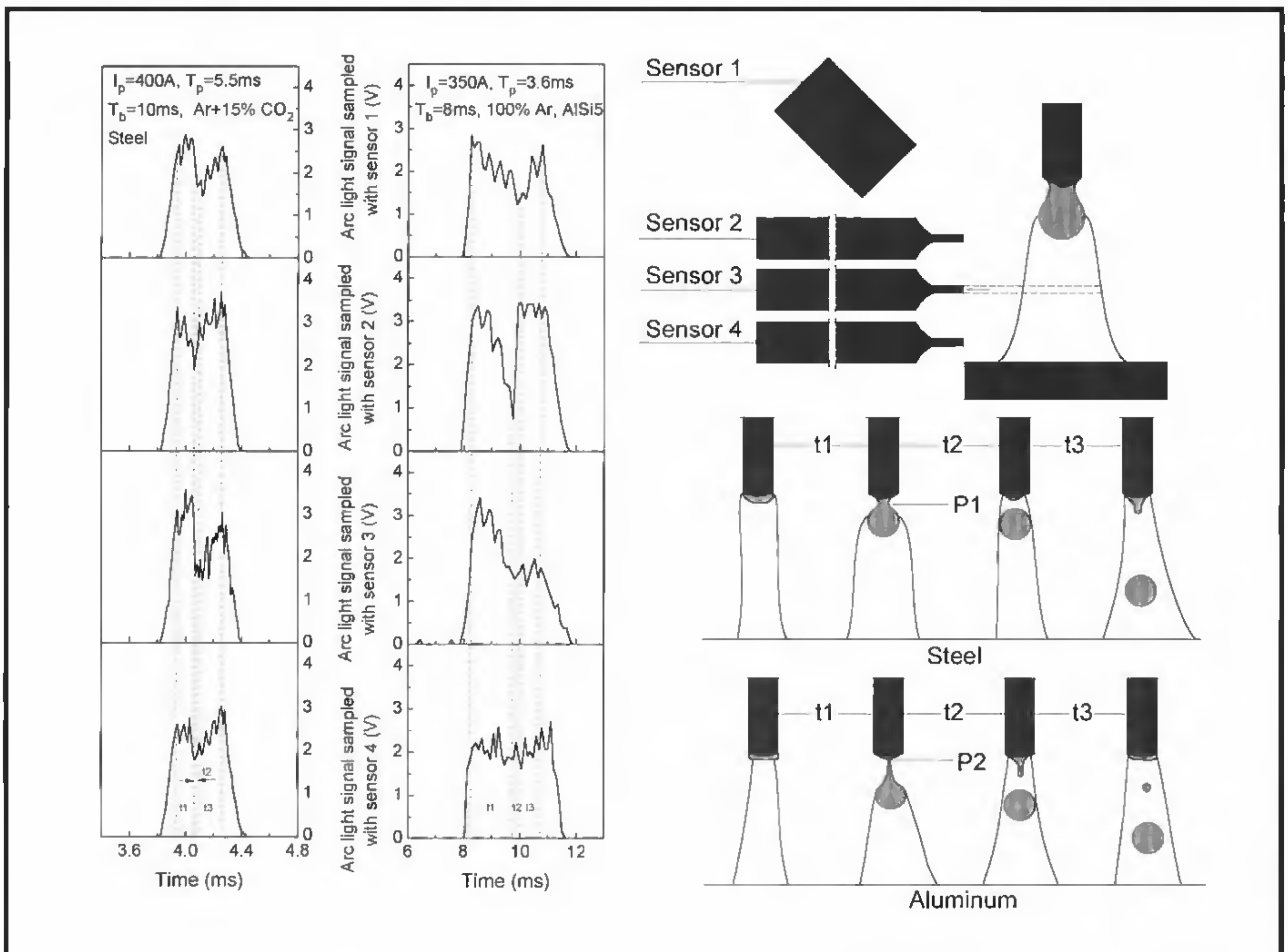

Fig. 15 — The schematic of sensing the arc light.

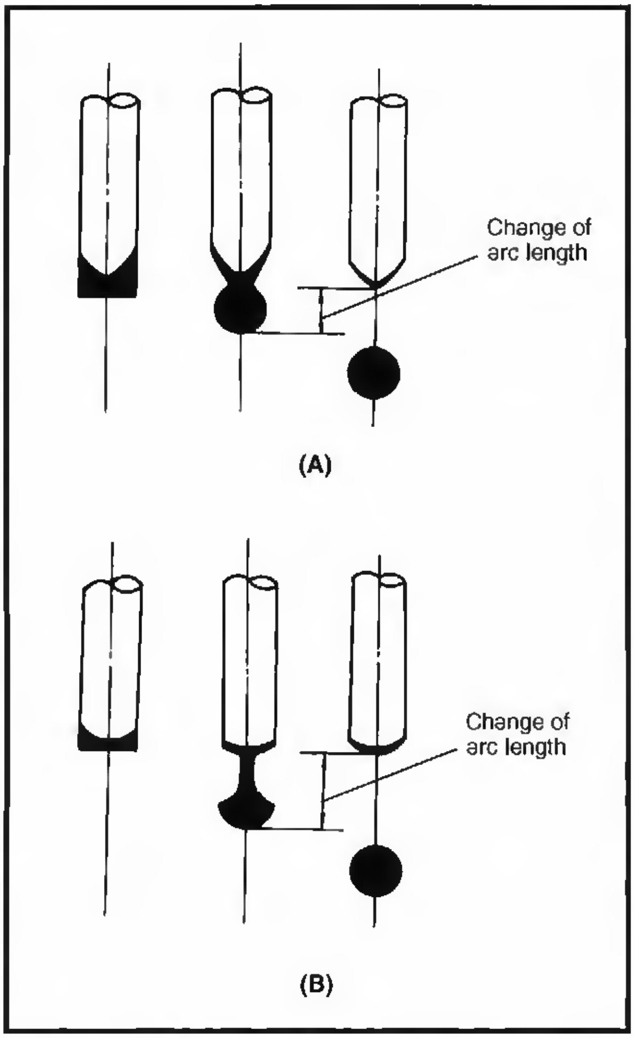

Fig. 16 — The melting behavior of the metal at the tip of the electrode. A — Steel; B — aluminum.

other. During the t1 period, with the enlargement of steel arc plasma luminary, the arc light signals collected by Sensors 3 and 4 increased gradually. In the aluminum alloy welding process, the change in arc length was largely due to the prolonged neck. Therefore, arc light radiant flux signal collected by Sensor 3 was also influenced by the change of arc length and decreased gradually. No obvious change occurred in the arc light signal collected by Sensor 4 because of no obvious change in arc radius. During the t2 period, in the steel welding process, the arc light signal collected by Sensors 3 and 4 decreased rapidly due to the abrupt constriction of the plasma luminary caused by droplet detachment. In aluminum alloy welding process, no obvious change occurred in the arc light signal collected by Sensors 3 and 4. During the t3 period, the arc plasma luminary of steel enlarged gradually, resulting in the increase of arc light signal collected by Sensors 3 and 4. In the aluminum alloy welding process, the arc light collected by Sensor 3 increased and that collected by Sensor 4 did not show any obvious change. Through the above experiments, we can conclude that the characteristic variation that indicates droplet detachment in steel arc light radiant flux signal depends largely upon the variation of plasma luminary radius. It has the same pattern as that of the signal collected by Sensor 3. The characteristic variation that indicates droplet detachment in aluminum alloy arc light radiant flux signal depended largely upon the arc length variation. It has the same pattern with that of the signal collected by Sensor 2.

Discussion

The Analysis of the Difference Between the Characteristic Arc Light Signal of Steel and that of Aluminum Alloy

As shown in the above experiments, arc light radiation from each part of the arc was different because of the different physical characteristics of steel and aluminum alloy. This led to the great difference of the entire arc light radiant flux signal between steel and aluminum alloy. The characteristic variation which indicated droplet transfer in steel arc light decreased rapidly due to droplet detachment, and increased gradually after droplet detachment. The characteristic variation that indicated droplet transfer in aluminum arc light decreased gradually before droplet detachment and increased rapidly after droplet detachment.

It can be deduced that the variation of arc light radiant flux signal of steel largely depends on the variation in the radius of the arc plasma luminary, and that of aluminum largely depends on variation of the arc length. The difference between them results from the different arc and droplet transfer behaviors, that is, different changes in arc length and radius of plasma luminary, which results from the different physical properties of steel and aluminum.

The different physical properties of steel and aluminum first result in significant differences between their arc temperatures. The thermal conductivity, specific heat and melting heat of steel are all lower than that of aluminum, as shown in Table 1. The temperature of the steel arc is relatively low (6000–8000 K) (Ref. 30). The steel arc is mainly composed of argon and iron vapor. If I_{Ar} and I_{Fe} are defined as spectrum line intensities of argon and iron, N_{Ar} and N_{Fe} are defined as the contents of argon and iron vapor in the arc, the following equation is fulfilled (Ref. 35):

$$I_{Ar} = N_{Ar} \cdot F_{Ar}(Te)$$
$$I_{Fe} = N_{Fe} \cdot F_{Fe}(Te) \qquad (8)$$

where $F_{Ar}(Te)$ and $F_{Fe}(Te)$ are the increasing function of electron temperature (less than 20,000 K). At the temperature of the steel arc the spectrum line intensity of argon, which is difficult to excite, is much lower than that of iron vapor, which is relatively easy to excite (Ref. 35). For this reason, the iron vapor content dominates the arc light radiant flux of the whole arc column. According to Equation 8, in order to maintain the light intensity when the content of iron vapor decreases, the electron temperature should be raised. The radial distribution of arc temperature is the decreasing function of radius (Ref. 30). Therefore, the radius of the plasma luminary with identical light intensity is an increasing function of iron vapor content in the arc. When the content of iron vapor increases, the radius of plasma luminary increases, and vice versa. The radius of the plasma luminary will affect the radiant flux of arc light according to Equation 5.

The temperature of the aluminum arc can be 21,000 K (300 A) or even higher (Refs. 30, 36), which is much higher than that of the steel arc. At this high temperature, with the exciting density of argon and aluminum atoms saturated, the difference in exciting potential between them is not dominant. Therefore, the characteristic variation in arc light radiant flux signal largely results from a change in the arc length.

On the other hand, different physical properties between steel and aluminum cause the geometric shape of the electrode tip to be different during the melting process, resulting in different changes in arc length. In welding process with direct current electrode positive, the melting part of the electrode tip is like the dark part in Fig. 16. Surrounded by molten metal, the solid part of the steel electrode tip represents a reverse conic shape due to the lower thermal conduc-

Table 1—Physical Properties of Steel and Aluminum

Physical Properties	Unit	Steel	Aluminum
Thermal conductivity	W/(cm·k)	0.32–0.66*	1.2–2.1*
Specific heat	J/(g·K)	0.763* (1810 K)	1.25* (933 K)
Melting heat	J/g	271.9	399.6
Coefficient of surface tension	10^{-3}N/m	1030	900
Resistivity	μΩ·cm	110 (1070 K)	10.9 (923 K)

Note * abstracted from AWS Handbook (Ref. 33); others from Ref. 34.

tivity of steel, and the outer molten metal gradually forms the pendant droplet. Because the lower part of the pendant droplet is heated continuously and its heat conduction is poor, its surface reaches the vaporizing point and becomes the main source of metal vapor emission. During the neck elongation, the arc length decreases and the metal vapor density increases, resulting in the increase of the radius of arc plasma luminary. Because the influence of metal vapor is dominant, arc light radiant flux signal increases gradually during the t1 period. During the t2 period, as soon as the neck breaks at the P1 point (Fig. 15), the arc roots jump from the lower surface of the detached droplet to the electrode tip. The arc length increases abruptly, resulting in an increase of the arc light radiant flux at the upper part of the arc. Because this change in arc length is not large — about 70–90% of the electrode diameter — the increase of arc light resulting from it is small. At the same time, the metal vapor source under the lower part of the droplet is suddenly eliminated after detachment, the plasma luminary constricts rapidly, resulting in the rapid decrease of the arc light radiant flux of the whole arc column. After the detachment of the droplet, the new source of metal vapor is formed on the wire tip and the metal vapor density in the arc then gradually increases again with gradual extension of the arc root on the wire tip surface. That is the formation process of the characteristic variation in arc light signal indicating the detachment of steel droplet detachment. The arc light radiant flux also increases with it.

Different from that of steel, the solid electrode tip of the aluminum alloy represents an obtuse shape, due to the higher heat conductivity, as shown in Table 1. For this reason, the vertical fraction of surface tension is relatively high. Due to good plasticity, the neck part is much longer and the arc length variation is much greater than that of steel with the same contact-tube-to-work distance, as shown in Fig. 16. Because the metal vapor content is not dominant in the aluminum arc, the arc light radiant flux decreases gradually with the gradual decrease of arc length. Just before the droplet detachment, the arc light signal reaches a minimum value. Once the droplet detaches, the arc root will jump from the droplet bottom up to the wire neck surface, which causes a larger change in arc length (150–200% of wire diameter). As a result, the increase of arc light signal is large and abrupt after the droplet detachment. This may be the reason for the different appearance of the characteristic signal of the aluminum droplet detachment.

The Influence of Shielding Gas on Arc Light Signal

The characteristic arc light signal indicating the droplet detachment in steel pulsed GMAW discussed above occurs only with argon-rich shielding gases (Ar-CO_2, Ar-O_2). However, when using pure argon as shielding gas and maintaining other welding parameters, no obvious variation in arc light radiant flux signal can be discriminated to indicate droplet detachment (Fig. 4C). This phenomenon shows there is a close relationship between shielding gas and characteristic arc light signal. Shielding gases influence the gradient of arc potential of arc column and change the behavior of arc and droplet transfer, resulting in the change of arc light radiant signal.

When the CO_2 content is below 5% in argon-rich shielding gas (Ar-CO_2), the characteristic variation of droplet detachment in arc light radiant flux signal is not obvious; this variation becomes obvious only when the CO_2 content in shielding gas is higher. In the steel welding arc with low CO_2 content, arc roots can climb up from the lower surface of droplet to the electrode tip above the neck before droplet detachment. According to the principle of minimum voltage, the new arc current channels after the arc roots climb should consume less energy than that of the original one, that is, the following expression (see Appendix for derivation) should be fulfilled:

$$\frac{I \cdot \rho}{\pi r_n^2} > E \tag{9}$$

where r_n is the radius of the neck, ρ is the specific resistance of molten metal, and E is the arc potential gradient of arc column. As shown in Table 1, the specific resistance of molten iron is high. When pure argon shielding gas is used, E is relatively lower. Therefore, according to Equation 9, the arc root can jump to the upper part of the neck easily and stay there for a relatively long time before droplet detachment. The neck gradually becomes the main metal vapor source. The reacting forces of vaporization press the neck to be a long liquid column until it breaks (Ref. 30). During this process, the droplet is enveloped by the arc column; thus, the arc length and metal vapor density do not change obviously due to droplet detachment, and no characteristic arc light signal will occur.

When argon-rich shielding gases are used, E is relatively higher than in Equation 9, and is difficult to fulfill. The arc roots are forced to constrict under the lower surface of the droplet, which becomes the main metal vapor emitting source. The arc roots jump to the upper part of the neck only when the neck becomes very thin (radius r_n is very small) and stay there only for a short time before droplet detachment. Because of the thermal inertia, the wire tip cannot immediately produce as much metal vapor at the lower part of the droplet as the previous metal vapor source was capable of producing. Therefore, the metal vapor density will decrease after droplet detachment. The higher the CO_2 or O_2 content in the shielding gas, the shorter the time the arc roots stay at the upper part of the neck before droplet detachment; thus, the greater the variation of metal vapor density appears, the greater the characteristic arc light signal will be. When density of CO_2 or O_2 in shielding gas reaches certain value (*i.e.*, CO_2 content is 35%), the change of the density of metal vapor caused by droplet detachment reaches its maximum, so the value of the characteristic signal does not increase any longer.

In aluminum welding with pulsed or steady current, Equation 9 is always difficult to fulfill due to the low specific resistance of aluminum alloy, as shown in Table 1. Arc roots cannot climb from the lower part of the droplet to the wire tip. Therefore, only the remarkable arc length variation caused by droplet detachment results in an obvious change in the arc light radiant flux signal. This sensing method is suitable both for pulsed and steady current GMAW of aluminum alloy.

Conclusion

1) The corresponding relationship between arc light radiant flux signal and droplet transfer in pulsed GMAW of steel and aluminum alloy was revealed.

2) A novel practical arc light sensing system was developed. The system can reliably detect droplet detachment in steel pulsed GMAW with argon-rich shielding and aluminum alloy GMAW with steady or pulsed current. The reliability is proven to be 96% and the maximal droplet detachment frequency that can be detected by this system is at least 130 Hz.

3) A closed-loop droplet transfer control system with arc light sensing was developed for pulsed GMAW of steel. The welding process with this control system is stable, quiet, spatter free and good weld formation is acquired.

4) A mathematical model of the arc light radiation was established. With the help of this model, the mechanism of variation of the arc light radiant flux signal caused by droplet detachment can be better understood.

5) One possible explanation for the different arc light characteristic signal of the droplet detachment in steel and aluminum alloy in pulsed GMAW is explained. The characteristic signal of steel is mainly determined by the variation of arc plasma luminary radius and that of aluminum by the variation of the arc length.

6) The influence of different shielding gases on the formation of the characteristic signal was discussed.

References

1. Santos, J. F. 1991. Metal transfer in consumable electrode arc welding — time for a reassessment. *IIW Doc.*, No. 212-780-91: 1–11.

2. Liu, S., Siewert, T. A., and Lan, H. 1989. Metal transfer mode in gas metal arc welding. *Proc. of the 2nd International Conf. on Trends in Welding Res.*: 475–479. May 14–18, Gatlinburg, Tenn.

3. Lahnsteiner, R. 1994. Advanced synergic inverter power source and wire-feed system for GMA welding with integrated quality control system. *Proc. International Conf. on Advanced Techniques and Low Cost Automation*: 204–213. September 5–6, Beijing, China.

4. Ueguri, S., Hara, K., and Komura, H. 1985. Study of metal transfer in pulsed GMA welding. *Welding Journal*, 64(8): 242-s to 250-s.

5. Collard, J. F. 1988. Adaptive pulsed GMAW control: The Digipulse system. *Welding Journal* 69(11): 35–38.

6. Matsui, H., and Suzuki, H. 1990. The effects of current wave shape and electrode wire contents on metal transfer in high speed pulsed MAG welding. *IIW Doc.*, No. 212-752-90: 104–116.

7. Ma, J., and Apps, R. L. 1983. New MIG process results from metal transfer mode control. *Welding & Metal Fabrication* 51(4): 168–175.

8. Dutra, J. C. 1990. Computerized procedure of metallic drop transfer analysis for the determination of pulsed welding variables. *IIW Doc.*, No. XII-1171-90: 234–244.

9. Kim, Y.-S, and Eagar, T. W. 1993. Metal transfer in pulsed current gas metal arc welding. *Welding Journal* 74(7): 279-s to 287-s.

10. Wang, Q. L., and Zhang, L. 1990. The research of synergic pulsed welding power supply. *Joining and Cutting*, 8: 1–7.

11. Uegari, S. 1984. United States Patent, 4438317.

12. Willgoss, R. A. 1984. Mathematical model predicts equilibrium. *Welding & Metal Fabrication* 52(9): 340–351.

13. Johnson, J. A., Carlson, N. M., Smartt, H. B., and Clark, D. E. 1991. Process control of GMAW: Sensing of metal transfer mode. *Welding Journal* 72(4): 91-s to 99-s.

14. Johnson, J. A., Carlson, N. M., and Smartt, H. B. 1989. Detection of metal transfer mode in GMAW. *Proc. 2nd International Conf. on Trends in Welding Res.*: 377–381. May 14–18, Gatlinburg, Tenn.

15. Chen, J. H., Fan, D., He, Z. Q., Ye, J., and Luo, Y. C. 1989. A study of the welding mechanism for globular metal transfer from covered electrodes. *Welding Journal* 70(4): 145-s to 150-s.

16. Clark, D. E., Buhrmaster, C. L., and Smartt, H. B. 1989. Drop transfer mechanisms in GMAW. *Proc. 2nd International Conf. on Trends in Welding Res.*: 371–375. May 14–18, Gatlinburg, Tenn.

17. Wang, Q. L. 1981. The study on the relation between arc sound and arc phenomena. *Science Report of Harbin Institute of Technology* 78(9): 124–129.

18. Madigan, R. B., Quinn, T. P., and Siewert, T. A., 1989. Sensing droplet detachment and electrode extension for control of gas metal arc welding. *Proc. 3rd International Conf. on Trends in Welding Res.*: 999–1002. Gatlinburg, Tenn.

19. Araya, T., and Endo, Y. 1981. Study on pulse current MIG welding of aluminum. *Journal of the Japan Welding Society* 50(2): 75–81.

20. Gulsoz, A., and Rehfeldt, D. 1991. Melting behavior of basic electrodes in direct and alternating current welding. *IIW Doc.*, No. 212-780-91.

21. Zhang, L. 1991. Arc light sensing and real-time control of droplet transfer in pulsed MIG (MAG) welding. Ph.D. dissertation, Harbin Institute of Technology.

22. Adam, G., and Siewert, T. A. 1990. Sensing of GMAW droplet transfer modes using an ER100s-1 electrode. *Welding Journal* 71(3): 103-s to 108-s.

23. Needham, J. C., 1985. What do you mean by voltage? *The Welding Institute Research Bulletin* 26(9): 311–316.

24. Heald, P. R., Madigan, R. B., Siewert, T. A., and Liu, S. 1994. Mapping the droplet transfer modes for an ER100s-1 GMAW electrode. *Welding Journal* 75(2): 38-s to 44-s.

25. Trindade, E. M., and Allum, C. J. 1984. Characteristics in steady and pulsed current GMAW. *Welding & Metal Fabrication* 52(8): 264–272.

26. Ohshima, K., Abe, M., and Kubota, T. 1982. Sampled-data control of arc length in MIG pulsed arc welding. *The Journal of Japanese Welding Institute* 51(8): 82–89.

27. Wang, Q. L., and Zhang, L. 1992. Arc light sensing of droplet transfer in GMA welding and the real-time control of one pulse one droplet. *Proc. 40th Annual Conf. of the Welding Technology Institute of Australia*: Vol. 1. June 29–July 3.

28. Song, Y. L. 1991. Spectroscopic study and its application in welding arc plasma. Ph.D. dissertation, Harbin Institute of Technology, China.

29. Song, Y. L., and Li, J. Y. 1995. Thermoequilibrium in welding arc plasma. *Transactions of China Welding Institution* 15(2): 138–145.

30. Ando, K. 1985. *Arc Physical Phenomena*. Mechanical Industry Press, Beijing, China.

31. Guo, Z. Y. 1986. *Arc and Thermal Plasma*. Science Press, Beijing, China.

32. Derliesven, C. B. 1980. *Physics and Technology of Gas Discharging*. Science Press, Beijing, China.

33. 1991. *AWS Welding Handbook*, Vol. 2. American Welding Society, Miami, Fla.

34. Zhou, Z. F. 1980. *Welding Metallurgy and Weldability of Metal*. Mechanical Industry Press, Beijing, China.

35. Bochikov, O. 1958. *The Spectrum Analysis of the Gas Mixture*. Science Press, Beijing, China.

36. Lancaster, J. F. 1984. *The Physics of Welding*, p. 171, Pergamon Press.

Appendix

a) According to the principle of Ohm with differential pattern:

$$j_r = \sigma E \tag{1a}$$

where j_r is current density, σ is electric conductivity, E is the voltage gradient of arc. By substituting j_r in Equation 4 in the paper we obtain:

$$j_r E = -\frac{1}{r} d\left(\frac{r\lambda dT}{dr}\right)/dr \tag{2a}$$

It is now assumed that λ is constant; by integrating T in Equation 2a, we obtain:

$$T = -\frac{IEr^2}{4\pi R^2 \lambda} + C_1 \tag{3a}$$

where C_1 is a constant. By substituting T in Equation 3 in the paper, we obtain:

$$U_v = 8\pi k \frac{v^2}{c^3}\left(-\frac{IEr^2}{4\pi R^2 \lambda} + C_1\right) \tag{4a}$$

When $r > ra$, $\sigma = 0$, Equation 4 in the paper can be converted to:

$$\lambda dT = -\frac{IE}{2\pi r} dr \tag{5a}$$

By integrating T in Equation 5a, we obtain:

$$T = -\frac{IE \ln r}{2\pi \lambda} + C_2 \tag{6a}$$

where C_2 is a constant. By substituting T in Equation 3 in the paper, we obtain:

$$U_v = 8\pi k \frac{v^2}{c^3}\left(-\frac{IEr^2}{4\pi R^2 \lambda} + C_2\right) \quad (7a)$$

The radiant flux ϕ can be obtained by differentiating arc radiant energy with respect to time. The rule of the variation of arc radiant flux can be analyzed by analysis of radiant energy. It is now assumed that arc column is an optical lamina that does not absorb radiant energy. By integrating U_v over volume, we obtain the radiant energy of the whole arc column, R_L is defined as the radius of plasma luminary:

$$\begin{aligned} U &= \iiint U_v dv = \int_0^L \iint U_v dS dl = L \iint U_v dS \\ &= L\left(\int_0^{r_a} 2\pi r U_v dr + \int_{r_a}^{R_L} 2\pi r U v dr\right) \\ &= 8\pi k \frac{v^2}{c^3}\left\{IEL\left[\left(\frac{1}{4} - \frac{\ln R_L}{2}\right) R_L^2 \right.\right. \\ &\left.\left. + \left(\frac{\ln r_a}{2} - \frac{3}{8}\right) r_a^2\right] \right. \\ &\left. + \pi C_2 L R_L^2 + \pi C_3 L r_a^2 \right\} \end{aligned} \quad (8a)$$

where U is the radiant energy of the whole arc column within unit frequency interval, C_3 is a constant. Considering other radiant sources, such as the welding pool, and energy loss to some extent, a constant C should be added to the calculated result. Thus, U can be represented as

$$\begin{aligned} U &= 8\pi k \frac{v^2}{c^3}\left\{IEL\left[\left(\frac{1}{4} - \frac{\ln R_L}{2}\right) R_L^2 \right.\right. \\ &\left.\left. + \left(\frac{\ln r_a}{2} - \frac{3}{8}\right) r_a^2\right] \right. \\ &\left. + \pi C_2 L R_L^2 + \pi C_3 L r_a^2 \right\} + C \end{aligned} \quad (9a)$$

b) According to the principle of minimum voltage, when the arc roots climb to the electrode tip above the neck from the droplet bottom, it should be fulfilled that

$$\frac{U_n}{L_n} > E \quad (1b)$$

where U_n is the potential across the neck, L_n is the length of the neck, E is the voltage gradient of the arc column. It is now assumed that the neck is a liquid metal column with length of L. R_n is defined as the resistance of this liquid metal column, ρ is the resistivity of molten iron. Then U_n can be represented as

$$U_n = I \cdot R_n = \frac{I \cdot \rho \cdot L}{S} = \frac{I \cdot \rho \cdot L_n}{\pi r_a^2} \quad (2b)$$

By substituting U_n in Equation 1b, we obtain:

$$\frac{I \cdot \rho}{\pi r_a^2} > E \quad (3b)$$